


Article

Study on the Coarsening Behavior of Interphase Precipitates and Random Precipitates in Steel Under the High-Temperature Environment of Fire

Jinghua Cong ^{1,†} , Yongzhe Yang ^{1,†}, Haibin Zhu ¹, Xueliang Shang ¹, Hongyu Wu ¹, Zhendong Song ², Xuemin Wang ^{1,*} and Xiangyu Xu ^{3,*}

¹ Collaborative Innovation Center of Steel Technology, University of Science and Technology Beijing, Beijing 100083, China; congjinghua@126.com (J.C.); yangyongzhe0812@163.com (Y.Y.); haibinzhu123@163.com (H.Z.); shangxl1996@163.com (X.S.); whymomei@sina.cn (H.W.)

² Technical Center of Inner Mongolia Baotou Steel Union Co., Ltd., Baotou 014010, China; szhd1982@126.com

³ Center for Advanced Solidification Technology, School of Materials Science and Engineering, Shanghai University, Shanghai 200444, China

* Correspondence: wxm@mater.ustb.edu.cn (X.W.); xuxiangyu@shu.edu.cn (X.X.)

† These authors contributed equally to this work.

Abstract: In the domain of fire-resistant steels, the characteristics of precipitates significantly influence material properties. This study developed a novel heat treatment protocol to concurrently achieve both interphase precipitation and random precipitation. Samples were subjected to isothermal treatments at various temperatures and durations, while techniques such as scanning electron microscopy (SEM) and transmission electron microscopy (TEM) were employed to thoroughly analyze the coarsening behavior of the two types of precipitate and reveal their thermal stability differences. The results show that the growth and coarsening rates of interphase precipitates are substantially lower than random precipitates. Coarsening kinetics analysis reveals that the radius of random precipitates follows a 1/3 power law with time at 600 °C and 650 °C, whereas the radius of interphase precipitates adheres to a 1/6 power law at 600 °C and a 1/5 power law at 650 °C. Furthermore, interphase precipitation demonstrates excellent size uniformity, which hinders the formation of a concentration gradient, thereby reducing the coarsening rate and enhancing thermal stability. After prolonged tempering treatment, interphase precipitation maintains a higher strengthening contribution than random precipitation. This study provides novel insights and theoretical foundations for the design and development of fire-resistant steels.

Keywords: interphase precipitation; random precipitation; thermal stability; coarsening behavior



Academic Editor: Frank Czerwinski

Received: 10 December 2024

Revised: 8 January 2025

Accepted: 14 January 2025

Published: 16 January 2025

Citation: Cong, J.; Yang, Y.; Zhu, H.; Shang, X.; Wu, H.; Song, Z.; Wang, X.; Xu, X. Study on the Coarsening Behavior of Interphase Precipitates and Random Precipitates in Steel Under the High-Temperature Environment of Fire. *Metals* **2025**, *15*, 73. <https://doi.org/10.3390/met15010073>

Copyright: © 2025 by the authors. Licensee MDPI, Basel, Switzerland. This article is an open access article distributed under the terms and conditions of the Creative Commons Attribution (CC BY) license (<https://creativecommons.org/licenses/by/4.0/>).

1. Introduction

The behavior of precipitates in steels plays a crucial role in determining the mechanical properties, high-temperature performance, and long-term durability of these materials [1–3]. These steels are widely used in demanding applications such as power plants, high-temperature reactors, and turbine components, where their ability to withstand elevated temperatures without significant degradation is critical [4–6]. Studies have shown that precipitate formation and coarsening during heat treatment processes are pivotal in optimizing steel properties by influencing the microstructure and controlling mechanisms such as creep resistance, oxidation resistance, and thermal stability [7–9]. Precipitation hardening in fire-resistant steels, or other steels requiring high-temperature performance,

is typically achieved through the formation of fine, stable precipitates, such as carbides, nitrides, and intermetallic compounds. However, prolonged exposure to high temperatures leads to the coarsening of these precipitates, which can result in a reduction in the steel's strength and resistance to deformation.

The coarsening of precipitates is a thermally activated process involving atom migration within the precipitate matrix, driven by differences in chemical potential between the precipitate and the surrounding matrix [6–9]. Understanding the mechanisms behind precipitate coarsening is essential for optimizing the performance of fire-resistant steels and other steels requiring high-temperature performance. Higher temperatures generally accelerate coarsening, and this relationship has been extensively studied in fire-resistant steels, where service conditions typically involve operation at elevated temperatures for extended periods. Studies have shown that the rate of precipitate coarsening depends on several factors, including temperature, alloying elements, and the initial size distribution of precipitates [10–13]. Wang [8] and Dudko [9] find that controlled heat treatments can significantly reduce precipitate coarsening, thereby enhancing the steel's strength at elevated temperatures. Furthermore, precipitate coarsening plays a crucial role in the creep behavior of these steels. Kesternich [14] and Miyata [15] find that creep resistance is closely linked to the size and distribution of precipitates, with finer precipitates effectively pinning grain boundaries and dislocations, thereby improving resistance to deformation under high-temperature stress. Therefore, a deeper understanding of the coarsening process and its influencing factors can inform the design of steels with superior performance in high-temperature environments.

Interphase precipitation, as a special type of precipitation, has garnered particular interest from researchers [16–18]. The contribution of interphase precipitation to strength at room temperature can reach approximately ~300 MPa [19]. Additionally, Yang's research finds that interphase precipitation plays a significant role in creep strengthening [20]. While substantial progress has been made in understanding the mechanisms of interphase precipitation and its role in strengthening, the high-temperature stability of these precipitates under service conditions remains largely underexplored. The stability of interphase precipitates at elevated temperatures is critical, as their coarsening or dissolution can result in the loss of the beneficial strengthening effect, particularly during long-term high-temperature exposure. Recent studies on precipitate coarsening have primarily focused on the bulk behavior of precipitates in alloys, without distinguishing between the precipitates formed during the phase transformation process and those formed in the bulk matrix. In contrast, the high-temperature coarsening behavior of interphase precipitates remains inadequately investigated. We have recently noted that interphase precipitation can effectively enhance the fire resistance of steels, primarily through precipitation strengthening and dislocation strengthening at elevated temperatures [21]. The aforementioned studies on interphase precipitation at elevated temperatures indirectly suggest that interphase precipitation exhibits excellent thermal stability.

In the present investigation, to investigate the thermal stability of interphase precipitation, a novel heat treatment method was developed to simultaneously induce both interphase and random precipitation at varying temperatures. Following isothermal treatments at different temperatures and durations, the coarsening behaviors and size uniformity of the two types of precipitate were analyzed to investigate the differences in their thermal stability and the underlying reason. The results of this study could provide an alternative approach to the design and development of fire-resistant steels.

2. Materials and Methods

Table 1 shows the chemical composition of the experimental steel measured using Inductively Coupled Plasma (ICP) and Inert Gas Fusion (IGF). The experimental steel was cast and rolled in the form of plate with a thickness of 14 mm. The experimental steel samples were homogenized in a quartz tube at 1200 °C for 72 h. Next, they were quenched in water. Thermo-mechanical treatments were then carried out using a continuous annealing simulator (ULVAC, Osaka, Japan). These heat treatment schedules are shown schematically in Figure 1. The sample after austenitizing at 950 °C and isothermal heat treatment at 650 °C is hereafter referred to as S0. The sample held at 600 °C for 1 h is hereafter referred to as S0-600 °C-1 h. Similarly, S0-600 °C-3 h and S0-600 °C-10 h are also named. The samples subjected to isothermal holding at 650 °C for different durations were labeled as S0-650 °C-1 h, S0-650 °C-3 h and S0-650 °C-10 h, respectively. SEM (scanning electron microscope) micrographs and TEM (transmission electron microscopy) micrographs were used to observe the precipitates. Specimens for microstructural studies were conducted using 3 mm diameter thin foils and mechanically thinned to 0.05 mm and electropolished using a solution of 5% perchloric acid and 95% alcohol at −25 °C. Then, a part of them was etched with 3% nital solution and observed using a JSM-7001F field emission scanning electron microscope (JEOL Ltd., Tokyo, Japan). To avoid statistical errors caused by thickness variations, SEM micrographs were used for the statistical analysis of the average diameter and density of precipitates, with a minimum of 20 images being analyzed in each specimen. Another part was used for confirmation of precipitate types by JEM-2100 TEM (JEOL Ltd., Tokyo, Japan). MATLAB software (R2021b) was used to programmatically process the SEM images of the precipitates, making them more accessible for observation, statistical analysis, and further interpretation. Microhardness measurements of ferrite were taken randomly using a Vickers hardness tester (CAS, Shanghai, China) with a load of 0.01 kg.

Table 1. The chemical composition of the experimental steel (wt.%).

C	Mn	Si	Ti	S	P	Fe
0.07	1.30	0.18	0.10	0.009	0.012	Bal.

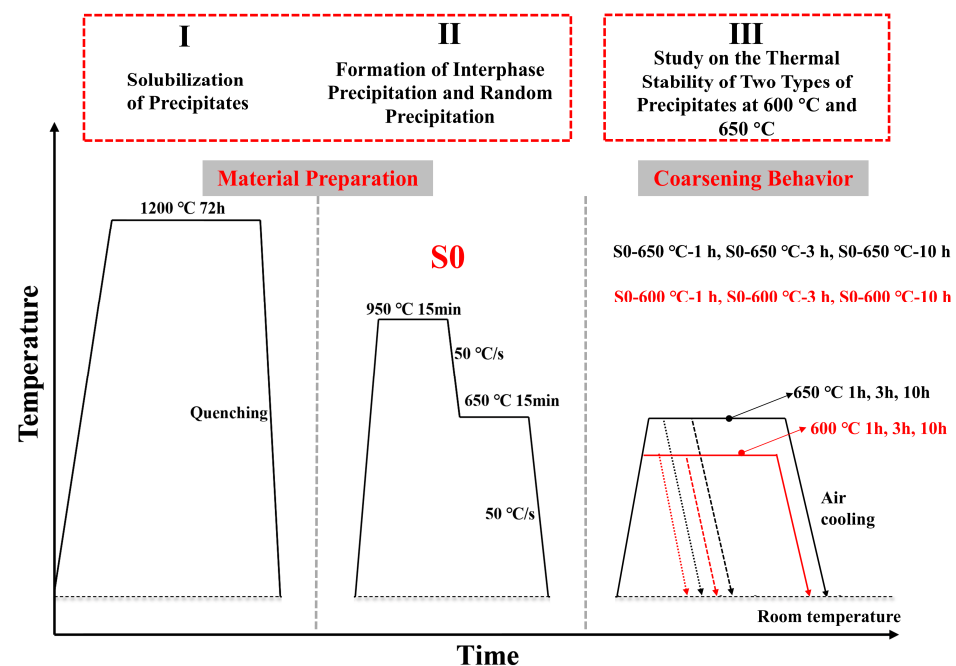


Figure 1. Schematic diagram illustrating the heat treatment process of the microalloyed steels.

3. Results

After being kept at a temperature of 1200 °C for a long period of time, the precipitated elements were basically all dissolved into the matrix. Then, after austenitizing at 950 °C and isothermal heat treatment at 650 °C, the microstructure shown in Figure 2 was obtained. The microstructure primarily consisted of ferrite, with a small amount of bainite present. This is consistent with the phase transformation behavior observed in the study [22]. The corresponding process is shown in stage II of Figure 1. During isothermal transformation at 650 °C, as described in the previous studies [23,24], due to the coordination of the moving speed of the front of the phase boundary and the enrichment of the precipitating elements on the slip planes of step planes, a large amount of interphase precipitation appeared during the early stage. However, it was difficult to observe interphase precipitation in the later stage, and a large amount of random precipitation occurred. After isothermal transformation at 650 °C for 15 min, the samples were subsequently held at 600 °C and 650 °C for 1 h, 3 h, and 10 h, respectively. The corresponding process is shown in stage III of Figure 1. At this stage, due to the higher diffusion rate and higher energy of grain boundaries, carbides tended to precipitate easily at the grain boundaries, resulting in a significant amount of precipitation at these locations [25]. However, this study primarily focuses on interphase and random precipitates within the grains and thus will not discuss this in further detail. The selection of these two temperatures was primarily based on the environmental temperatures encountered during the fire-resistant testing of the steel [26]. Through TEM observation and energy-dispersive X-ray spectroscopy (EDS) analysis, it can be seen that the precipitates in sample S0 were mainly interphase precipitation (as indicated by the white dashed lines in Figure 3a) and random precipitation (as indicated by the white circles in Figure 3a). The EDS analysis in Figure 3b confirms that the precipitates were primarily TiC, and previous research also verified that the carbide was the MC (M = Mo/Ti/V/Nb) carbide (Metallic Carbides) with an NaCl-type crystal structure, which will not be elaborated in this article [21–23,27,28].

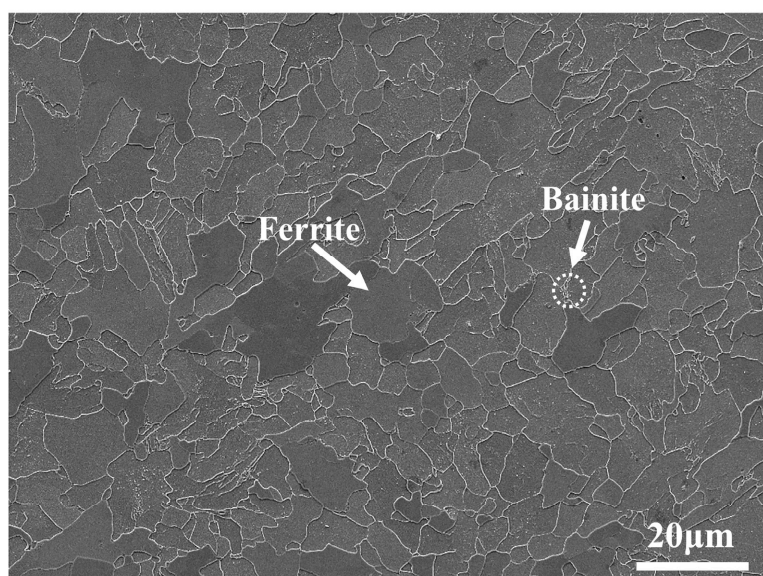


Figure 2. SEM micrographs of sample S0.

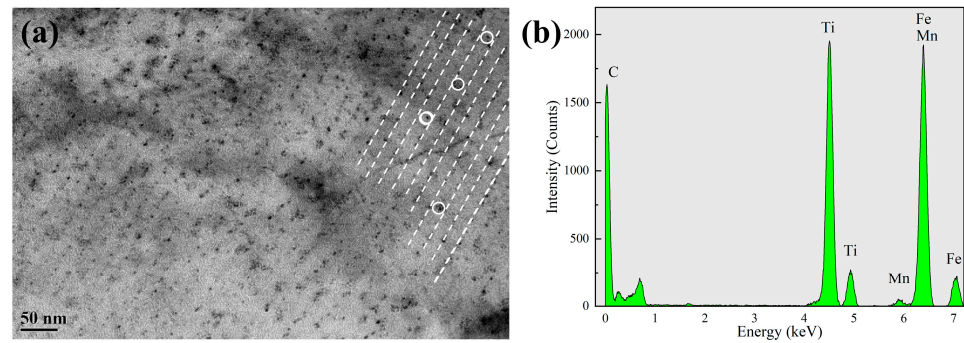


Figure 3. TEM micrographs (a) and EDS analysis (b) of the precipitates in sample S0.

In order to avoid the influence of thickness, SEM micrographs were used instead of TEM micrographs to observe the precipitates. Figures 4 and 5 present the SEM micrographs of precipitates at different holding times at 600 °C and 650 °C, along with corresponding images processed using the MATLAB program. We can observe that there are rows of interphase precipitation and random precipitation. The method of equivalent area circle was adopted to measure the size of the precipitates. A program written in MATLAB was utilized to count the number of pixel points of each independent precipitate (black spot) in the binarized image. The pixel count was then converted into the actual area using a calibration scale. Each precipitate was approximately regarded as a perfect circle, and its diameter was calculated based on the area, which was taken as the approximate diameter of the precipitate. Figures 4 and 5 clearly show that precipitate coarsening and growth occurred more slowly with partitioned precipitation compared to random precipitation. Additionally, higher temperatures accelerated this coarsening and growth process. After 10 h at 650 °C, the coarsening trend became particularly evident.

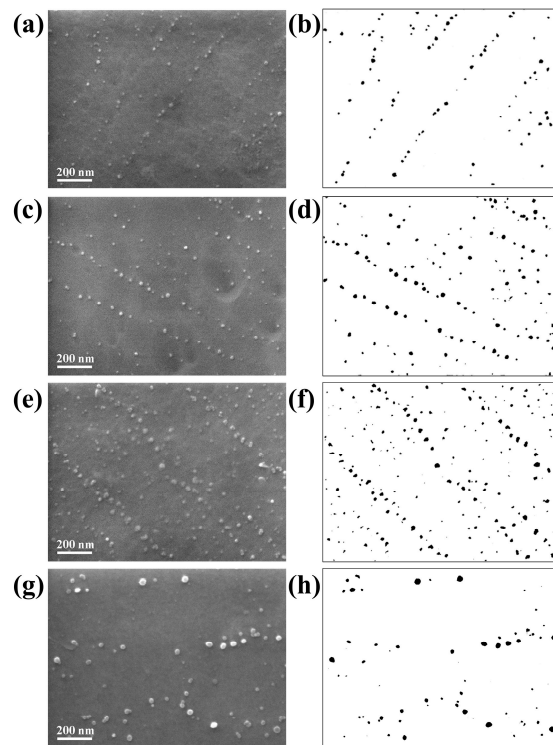


Figure 4. SEM micrographs (a,c,e,g) and binarized images (b,d,f,h) of precipitates with different isothermal holdings time at 600 °C in the microalloyed steels. (a,b) S0 (c,d) S0-600 °C-1 h, (e,f) S0-600 °C-3 h, (g,h) S0-600 °C-10 h.

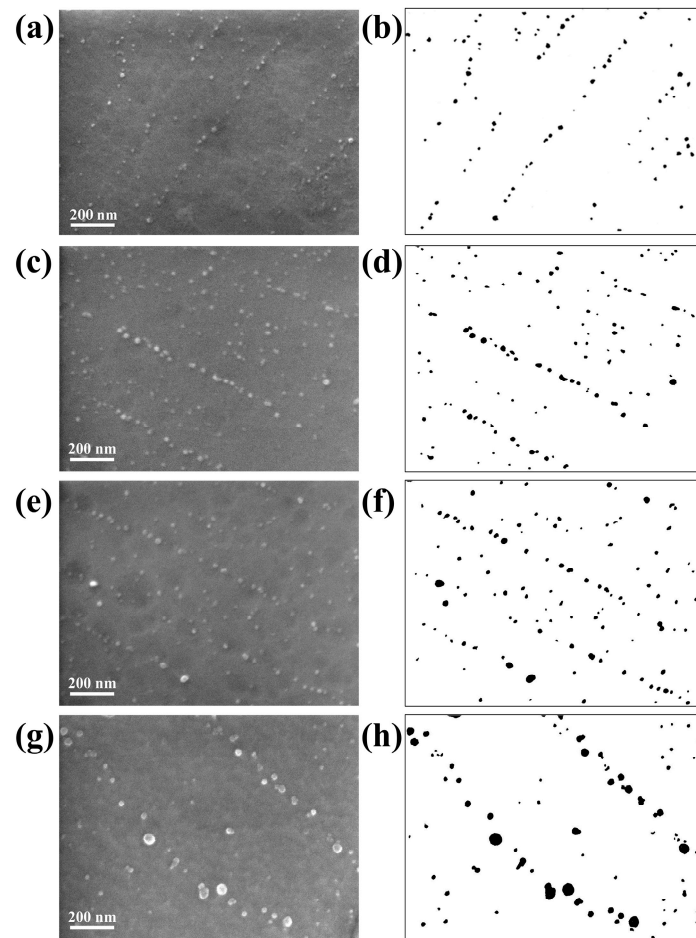


Figure 5. SEM micrographs (a,c,e,g) and binarized images (b,d,f,h) of precipitates with different isothermal holding times at 650 °C in the microalloyed steels. (a,b) S0, (c,d) S0-650 °C-1 h, (e,f) S0-650 °C-3 h, (g,h) S0-650 °C-10 h.

4. Discussion

4.1. Coarsening Kinetics

In order to investigate the coarsening behavior of different precipitates at various temperatures, it is essential to quantify the precipitate size at different holding times and temperatures. The precipitate size, represented by the equivalent circular diameter in this study, varies with the holding time, as shown in Figure 6. The error bars indicate the maximum and minimum values within the 99% confidence interval of the measured data.

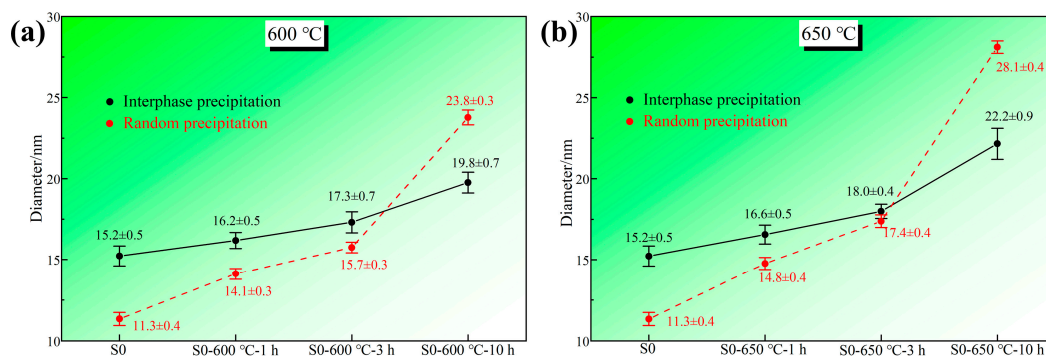


Figure 6. Variation of the average diameter of precipitates with different isothermal holding times at 600 °C (a) and 650 °C (b) in the microalloyed steels.

Interphase precipitation occurs at the phase boundary during the early stage of phase transformation when held at 650 °C for a period of time; its size is slightly bigger than random precipitation. According to statistical analysis, the average diameter of interphase precipitation of sample S0 was ~15.2 nm, while the random precipitation was ~11.3 nm. With the increase in holding time, the size of the interphase precipitates was gradually increased. The average diameter of the interphase precipitates was still only ~19.8 nm at 600 °C for 10 h, and increased by ~30%. The average diameter of the interphase precipitates was ~22.2 nm at 650 °C for 10 h, and increased by ~46%. This indicates that interphase precipitation is more likely to grow at 650 °C compared to 600 °C. In contrast, with the increase in holding time, the average size of random precipitates increased significantly at 600 °C, especially for 3 h to 10 h, and the average diameter increased by ~52%. During the initial three hours of the holding process, the precipitate size increased slowly. However, a noticeable acceleration in growth occurred after just one hour at 650 °C. From 1 and 10 h, the average diameter of the random precipitates grew by ~90%. Based on the above, interphase precipitation grew more slowly than random precipitation at both 600 °C and 650 °C, with no significant increase in average size over the entire 10-h period. In contrast, random precipitation at 600 °C exhibited a sharp increase in growth rate starting from 3 h. At 650 °C, this rapid growth phase began earlier, and the increase in growth rate was more pronounced.

The size of the precipitates shows a certain variation rule with time, and there is an equation proposed by some research on the variation of precipitate size with time [29].

$$\left(r_t^3 - r_0^3\right) = \frac{K}{RT} V^2 C D \gamma t \quad (1)$$

where, r_t and r_0 represent the average particle radius at time 0 and t , respectively; D is the diffusion coefficient of the solute in the matrix; γ is the interfacial energy between the precipitate and the matrix; C is the solute concentration at equilibrium; V represents the molar volume of the precipitate; and K is a constant.

To fit the exponential relationship between the precipitation radius and time, Equation (1) is simplified, using N as the time exponent and K' as the constant, to obtain Equation (2).

$$\left(r_t^N - r_0^N\right) = K' t \quad (2)$$

Based on the fitting results of Equation (2) shown in Figure 7, the time exponent for random precipitates at 600 °C is $N = 3$ with a correlation of 0.982, and the time exponent for interphase precipitates at 600 °C is $N = 6$ with a correlation of 0.999. According to the statistical results in this paper, the average size of the random precipitates at 600 °C follows the 1/3 power law of t , while the average size of the interphase precipitates at 600 °C is close to the 1/6 power law of t . Similarly, based on the fitting results of Equation (2) shown in Figure 8, the time exponent for the random precipitates at 650 °C is $N = 3$ with a correlation of 0.977, and the time exponent for the interphase precipitates at 650 °C is $N = 5$ with a correlation of 0.993. According to the statistical results in this paper, the average size of the random precipitates at 600 °C or 650 °C follows the 1/3 power law of t , while the average size of the interphase precipitates at 600 °C is close to the 1/6 power law of t and at 650 °C is close to the 1/5 power law of t . According to relevant theories, the 1/3 power law of t applies to the later stage of second-phase particle precipitation in a supersaturated solid solution, where the coalescence process plays a dominant role. At this stage, the supersaturation of the matrix becomes very small, and the growth of the grains occurs primarily through the incorporation of smaller grains by larger ones [30–32]. The 1/4 power law of t applies to the precipitates on the grain boundary and the 1/5 power law of t applies to the precipitates on dislocation [30–32]. During the coarsening process,

solute diffusion is governed by a characteristic distance related to the spatial distribution of the particles, which is influenced by the volume fraction of the precipitates [31,32]. Consequently, this affects the coarsening rate. It can be seen from the results that the exponent of the precipitate radius and time of random precipitates are consistent with those of supersaturated precipitates; the interphase precipitates are smaller than the precipitates on dislocation or the grain boundary; and the growth and coarsening rates of interphase precipitates are slower than that of random precipitates.

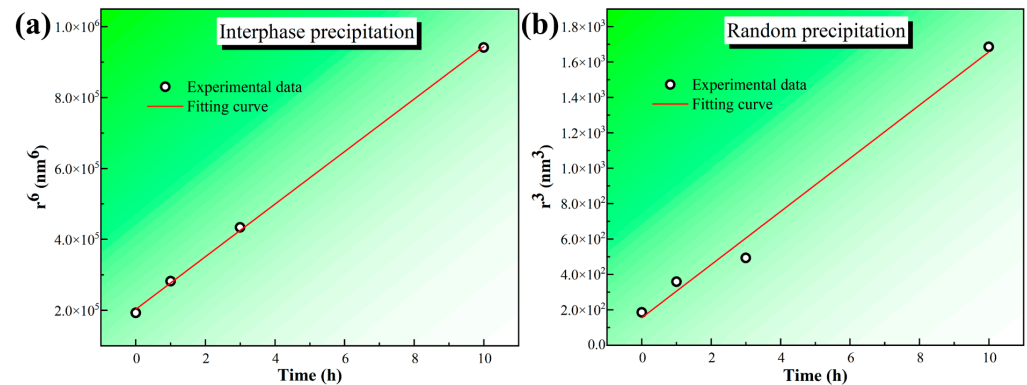


Figure 7. Plot of the mean radius of different precipitates against time at 600 °C: (a) is interphase precipitation; (b) is random precipitation.

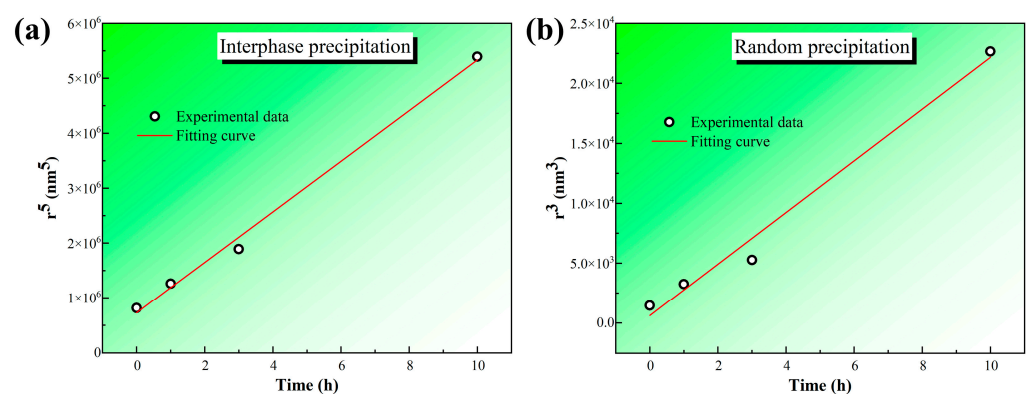


Figure 8. Plot of the mean radius of different precipitates against time at 650 °C: (a) is interphase precipitation; (b) is random precipitation.

4.2. The Effect of Precipitate Size Uniformity

As analyzed above, it can be seen that, whether at 600 °C or 650 °C, the growth and coarsening rates of interphase precipitation are significantly smaller than that of random precipitation. The same trend is observed during holding at both temperatures. Therefore, the following discussion will focus on analyzing the reasons behind the different growth and coarsening behaviors of the two types of precipitate at 600 °C.

First, an analysis will be conducted based on the density of the two types of precipitate. In view of the unique distribution, we adopted the linear density approach to determine the density of interphase precipitates. It can be seen from Figure 9 that the linear density of the interphase precipitates decreased from 3 h to 10 h at 600 °C, while the area density of the random precipitates decreased to a certain extent from 1 h to 3 h at 600 °C, and the decrease was more obvious after 3 h. Combined with the average diameter and density of precipitates, we can determine that the coarsening rate of interphase precipitates is significantly slower than that of random precipitates.

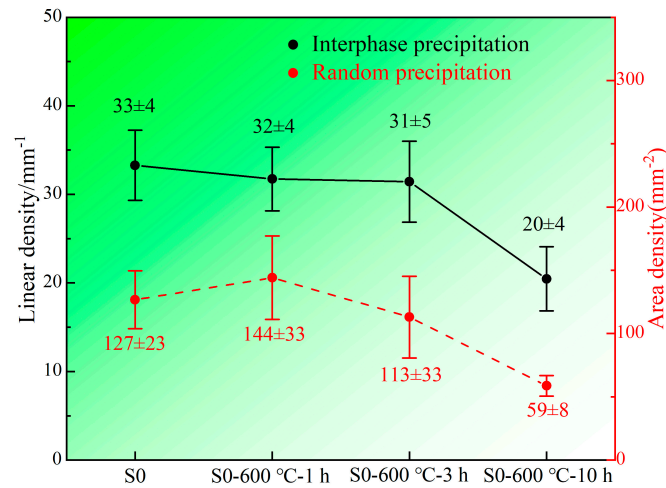


Figure 9. Variation of the average density of precipitates with different isothermal holding times at 600 °C in the microalloyed steels.

It is well known that interphase precipitation is formed on the slip planes of step planes of the phase boundary between ferrite and austenite. If the phase transformation temperature is constant, the size of the precipitates will be relatively uniform. If the phase transformation temperature is constant, the slip planes of step planes will disappear quickly, and the elements will not accumulate on it, which will lead to further growth of interphase precipitates. Thus, the size of the interphase precipitates is relatively uniform. However, due to the different formation times, the size difference of the random precipitates is obvious. From Figure 10, we can clearly identify that the full width at half maximum (FWHM) of the diameter distribution diagram of the interphase precipitates is significantly smaller than that of the random precipitates. The FWHM reflects the uniformity of precipitate sizes. A smaller FWHM indicates that the sizes of the precipitates within the statistical range are more consistent. Therefore, it can be concluded that the interphase precipitates have a more uniform size than the random precipitates.

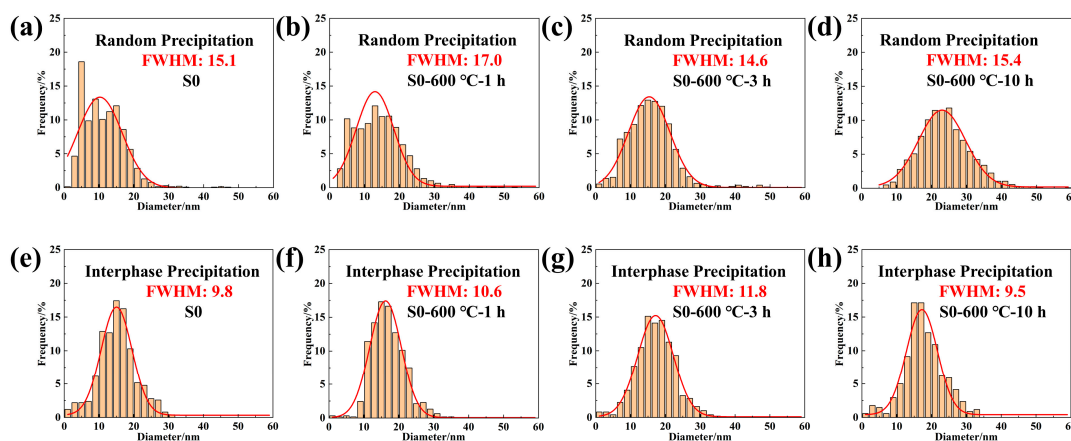


Figure 10. Distributions of precipitate diameter determined from the SEM images of the microalloyed steels held at 600 °C for various times: (a–d) are the statistical diagrams of random precipitation; (e–h) are the statistical diagrams of interphase precipitation (FWHM: the full width at half-maximum).

As is known to all, the coarsening of precipitates follows the Lifshitz–Slyozov–Wagner (LSW) theory [30,33]. LSW theoretical analysis is based on the Gibbs–Thompson equation, which is expressed by:

$$C_r = C_0 \exp \left[\frac{2\sigma V_m}{rRT} \left(\frac{1 - C_0}{C_p - C_0} \right) \right] \quad (3)$$

where C_r is the atomic fraction of solute in the matrix at the precipitate interfaces of radius r , σ is the specific interfacial energy of the matrix–precipitate boundary, V_m is the molar volume of the precipitate, C_0 is the equilibrium atomic fraction of Ti in the matrix, and C_p is the equilibrium atom fraction of Ti in the precipitates. The precipitate in this study is TiC, so the value of C_p is 1/2. However, the atomic fraction of Ti in the matrix is very low compared with that in the precipitates, and C_0 can be ignored. Thus, the exponential term can be simplified to $\frac{4\sigma V_m}{rRT}$. 4σ is ~ 1 J/m²; the order of magnitude of V_m is $\sim 10^{-5}$ m³/mol, and the order of magnitude of RT is $\sim 10^5$ J/mol. Therefore, when the radius of the precipitate is greater than 0.1 nm, $\frac{4\sigma V_m}{rRT}$ is less than 1; the exponential function can be expanded in power series and the high-order term can be omitted such that

$$C_r - C_0 \approx C_0 \left(\frac{4\sigma V_m}{rRT} \right) \quad (4)$$

From Equation (4), we can conclude that the smaller the size of precipitates, the higher the concentration of Ti in the precipitates. Figure 11 illustrates the differences in the size of the two types of precipitates and the atomic concentration profiles in their vicinity. The Ti atoms diffuse from the small-size precipitates to the large-size precipitates. This diffusion process destroys the concentration balance around the precipitates, resulting in the continuous dissolution and contraction of the small-size precipitates and the continuous growth of the large-size precipitates. However, the size distribution of the precipitates is uniform, and the concentration gradient does not occur easily. Accordingly, the coarsening rate of the interphase precipitates is slower than that of the random precipitates, and the thermal stability is higher.

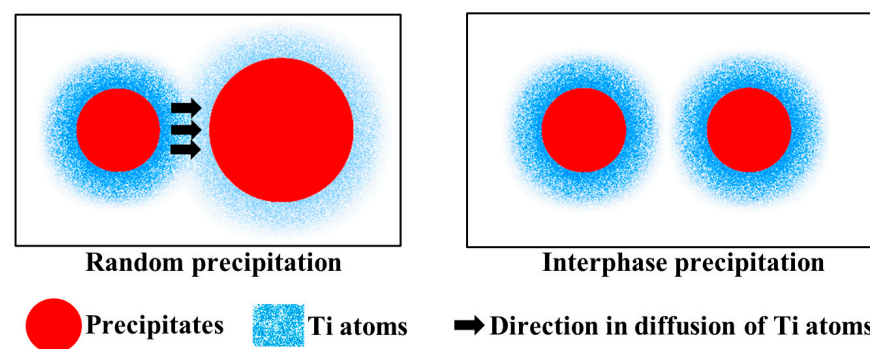


Figure 11. Schematic diagram of the diffusion of Ti atoms between interphase precipitation and random precipitation.

4.3. Properties and Evolution Behavior

Through observation and analysis, it can be seen that the coarsening growth rate of the interphase precipitates is slower than that of the random precipitates. The most important role of precipitates in steel is to strengthen through precipitation strengthening, and the level of the precipitation-strengthening contribution is mainly determined by the size and density of the precipitates. This paper estimates the precipitation-strengthening contribution $\Delta\tau_{\text{orowan}}$ through the Orowan–Ashby Equation (5) [34].

$$\Delta\tau_{\text{orowan}} = 0.26 \left(\frac{Gb}{r} \right) f^{1/2} \ln \left(\frac{r}{b} \right) \quad (5)$$

where G is the shear modulus (80,300 MPa) [35], r is the average radius of the precipitates (shown in Figure 6a), b is the Burgers vector (0.248 nm), and f is the area percentage of the precipitates (the volume percentage of the precipitates is converted based on the linear density and area density in Figure 9). The results are shown in Table 2.

Table 2. The volume fraction of precipitates and precipitation-strengthening contribution.

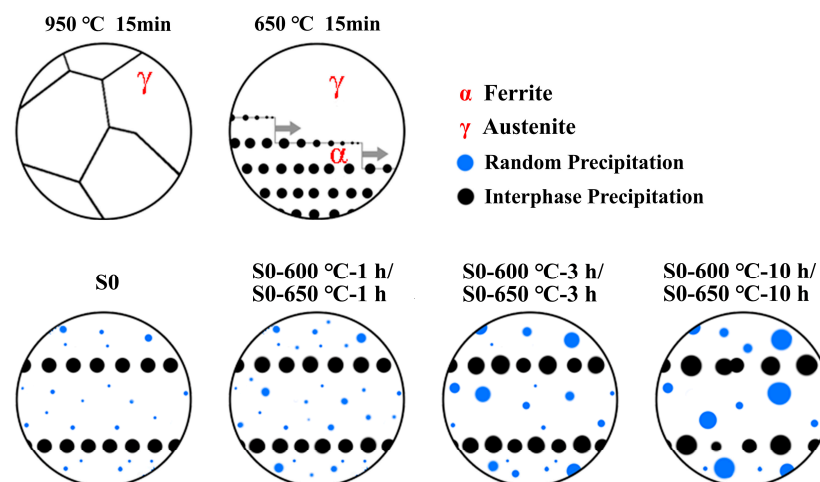
Type of Precipitates	f/%	S0	S0-600 °C-1 h		S0-600 °C-3 h		S0-600 °C-10 h	
		$\Delta\tau_{\text{orowan}}$	f/%	$\Delta\tau_{\text{orowan}}$	f/%	$\Delta\tau_{\text{orowan}}$	f/%	$\Delta\tau_{\text{orowan}}$
RP	0.027	47	0.03	42.9	0.024	35.2	0.012	18.8
IP	0.035	43.6	0.033	41	0.032	38.5	0.027	28.1

As shown in Table 2, in sample S0, although the volume fraction is small due to the smaller size of the random precipitates, the precipitation-strengthening contribution of random precipitation is higher than that of interphase precipitation. As the tempering time at 600 °C increases, the precipitation-strengthening contribution of random precipitation decreases substantially. Compared to its value before tempering, the precipitation-strengthening contribution of interphase precipitation decreases from ~43.6 MPa to ~28.1 MPa after 10 h of tempering, a reduction of ~35.6%, while that of random precipitation decreases by ~60%. The calculation results indicate that interphase precipitation maintains a higher precipitation-strengthening contribution after prolonged tempering compared to random precipitation. It is precisely due to the superior thermal stability of interphase precipitation that the hardness of the experimental steel did not decrease sharply with the increase in holding time at 600 °C. The results of microhardness measurements are presented in Table 3.

Table 3. The Vickers hardness values of different samples.

Sample	S0	S0-600 °C-1 h	S0-600 °C-3 h	S0-600 °C-10 h
HV0.01	181.7 ± 4.5	175.6 ± 1.3	176.6 ± 1.9	174.0 ± 1.5

In conclusion, we can clearly understand the precipitation processes of interphase precipitation and random precipitation from Figure 12. Additionally, it also illustrates the growth and coarsening rules of interphase precipitation and random precipitation under different tempering times. When held at 950 °C, it is completely transformed into austenite, and then at 650 °C, the ferrite phase transformation occurs, forming interphase precipitation. Afterwards, random precipitation is formed within the ferrite. During the subsequent holding process at 600 °C or 650 °C, the interphase precipitation has superior thermal stability than random precipitation, and its growth and coarsening rates are slower.

**Figure 12.** Schematic illustration of changes in the morphology and nature of precipitates during different processes.

5. Conclusions

In conclusion, this paper studies the thermal stability and coarsening behavior of interphase precipitation and random precipitation by analyzing the changes in size and density of different types of precipitate at elevated temperatures. The conclusions are summarized as follows.

- (1) At an elevated temperature, the coarsening rates of interphase precipitates are significantly lower than random precipitates. As the temperature increases, the coarsening of interphase precipitates progresses at a slower rate.
- (2) The coarsening behavior of random and interphase precipitates at 600 °C and 650 °C follows distinct power laws, with random precipitates adhering to a 1/3 power law and interphase precipitates following 1/6 and 1/5 power laws at 600 °C and 650 °C, respectively.
- (3) Interphase precipitation forms on the slip planes at the phase boundary and exhibits a uniform size, with an FWHM of 9.8, whereas random precipitation shows a pronounced size distribution due to varying formation times, with an FWHM of 15.1. The uniform size of interphase precipitates makes it challenging to form a concentration gradient, leading to slower coarsening and enhanced thermal stability.

Author Contributions: Conceptualization, X.W. and X.X.; Methodology, X.W. and X.X.; Software, H.Z., X.S. and Z.S.; Validation, H.W., X.W. and X.X.; Formal analysis, J.C., Y.Y. and H.W.; Investigation, J.C., Y.Y., H.Z., X.S. and Z.S.; Data curation, J.C., Y.Y., H.Z., X.S. and Z.S.; Writing—original draft, J.C. and Y.Y.; Writing—review & editing, H.W., X.W. and X.X.; Visualization, H.Z., X.S. and Z.S.; Supervision, X.W. and X.X. All authors have read and agreed to the published version of the manuscript.

Funding: This research was funded by the Science and Technological Plan Project in the Inner Mongolia Autonomous Region, grant number 2023YFHH0033.

Data Availability Statement: The original contributions presented in this study are included in the article. Further inquiries can be directed to the corresponding authors.

Acknowledgments: The authors are also grateful for the important assistance provided by Jiajie Fan.

Conflicts of Interest: Author Zhendong Song was employed by Technical Center of Inner Mongolia Baotou Steel Union Co., Ltd. The remaining authors declare that the research was conducted in the absence of any commercial or financial relationships that could be construed as a potential conflict of interest.

References

1. Xie, Z.; Song, Z.; Chen, K.; Jiang, M.; Tao, Y.; Wang, X.; Shang, C. Study of Nanometer-Sized Precipitation and Properties of Fire Resistant Hot-Rolled Steel. *Metals* **2019**, *9*, 1230. [[CrossRef](#)]
2. Kim, J.; Yu, G.; Kim, S.; Park, J.; Ahn, M.; Chung, J.-H.; Lee, C.-H.; Shin, C. Microstructural and Mechanical Characterization of Low-Alloy Fire- and Seismic-Resistant H-Section Steel. *Metals* **2024**, *14*, 374. [[CrossRef](#)]
3. Ferreira, P.P.; Carvalho, F.M.; Ariza-Echeverri, E.A.; Delfino, P.M.; Bauri, L.F.; Ferreira, A.M.; Braga, A.P.; Eleno, L.T.F.; Goldenstein, H.; Tschiptschin, A.P. Synergism between B and Nb Improves Fire Resistance in Microalloyed Steels. *Metals* **2023**, *13*, 84. [[CrossRef](#)]
4. Zhang, Z.; Niu, G.; Li, J.; Zhang, P.; Wu, H. Synergistic Effects of Ti and Mo on the Microstructure and Properties of Low-Cost Fire-Resistant and Weather-Resistant Construction Steel. *J. Mater. Eng. Perform.* **2023**, *32*, 3958–3967. [[CrossRef](#)]
5. Zhou, Y.; Liu, Y.; Zhou, X.; Liu, C.; Yu, J.; Huang, Y.; Li, H.; Li, W. Precipitation and Hot Deformation Behavior of Austenitic Heat-Resistant Steels: A Review. *J. Mater. Sci. Technol.* **2017**, *33*, 1448–1456. [[CrossRef](#)]
6. Wang, H.; Du, H.; Wei, Y.; Hou, L.; Liu, X.; Wei, H.; Liu, B.; Jia, J. Precipitation and Properties at Elevated Temperature in Austenitic Heat-Resistant Steels—A Review. *Steel Res. Int.* **2021**, *92*, 2000378. [[CrossRef](#)]
7. Zhang, Z.; Wang, Z.; Li, Z.; Sun, X. Microstructure Evolution and Precipitation Behavior in Nb and Nb-Mo Microalloyed Fire-Resistant Steels. *Metals* **2023**, *13*, 112. [[CrossRef](#)]

8. Wang, H.; Yan, W.; Van Zwaag, S.; Shi, Q.; Wang, W.; Yang, K.; Shan, Y. On the 650 °C Thermostability of 9–12Cr Heat Resistant Steels Containing Different Precipitates. *Acta Mater.* **2017**, *134*, 143–154. [[CrossRef](#)]
9. Dudko, V.; Belyakov, A.; Molodov, D.; Kaibyshev, R. Microstructure Evolution and Pinning of Boundaries by Precipitates in a 9 Pct Cr Heat Resistant Steel During Creep. *Metall. Mater. Trans. A* **2013**, *44*, 162–172. [[CrossRef](#)]
10. Jayanth, C.S.; Nash, P. Factors Affecting Particle-Coarsening Kinetics and Size Distribution. *J. Mater. Sci.* **1989**, *24*, 3041–3052. [[CrossRef](#)]
11. Martin, J.W. *Precipitation Hardening: Theory and Applications*; Butterworth-Heinemann: Oxford, UK, 2012.
12. Guo, Z.; Sha, W. Quantification of Precipitation Hardening and Evolution of Precipitates. *Mater. Trans.* **2002**, *43*, 1273–1282. [[CrossRef](#)]
13. Yin, Y.F.; Faulkner, R.G. Modelling the Effects of Alloying Elements on Precipitation in Ferritic Steels. *Mater. Sci. Eng. A* **2003**, *344*, 92–102. [[CrossRef](#)]
14. Kesternich, W.; Meertens, D. Microstructural Evolution of a Titanium-Stabilized 15Cr-15Ni Steel. *Acta Metall.* **1986**, *34*, 1071–1082. [[CrossRef](#)]
15. Miyata, K.; Sawaragi, Y.; Okada, H.; Masuyama, F.; Yokoyama, T.; Komai, N. Microstructural Evolution of a 12Cr-2W-Cu-V-Nb Steel during Three-Year Service Exposure. *ISIJ Int.* **2000**, *40*, 1156–1163. [[CrossRef](#)]
16. Funakawa, Y. Interphase Precipitation and Application to Practical Steels. *Mater. Trans.* **2019**, *60*, 2086–2095. [[CrossRef](#)]
17. Zhang, Y.; Shinbo, K.; Ohmura, T.; Suzuki, T.; Tsuzaki, K.; Miyamoto, G.; Furuhashi, T. Randomization of Ferrite/Austenite Orientation Relationship and Resultant Hardness Increment by Nitrogen Addition in Vanadium-Microalloyed Low Carbon Steels Strengthened by Interphase Precipitation. *ISIJ Int.* **2018**, *58*, 542–550. [[CrossRef](#)]
18. Wang, J.; Hodgson, P.D.; Bikmukhametov, I.; Miller, M.K.; Timokhina, I. Effects of Hot-Deformation on Grain Boundary Precipitation and Segregation in Ti-Mo Microalloyed Steels. *Mater. Des.* **2018**, *141*, 48–56. [[CrossRef](#)]
19. Funakawa, Y.; Shiozaki, T.; Tomita, K.; Yamamoto, T.; Maeda, E. Development of High Strength Hot-Rolled Sheet Steel Consisting of Ferrite and Nanometer-Sized Carbides. *ISIJ Int.* **2004**, *44*, 1945–1951. [[CrossRef](#)]
20. Yang, Y.-L.; Lin, Q.-X.; Chen, C.-Y.; Jen, Y.-M.; Wang, S.-H.; Chen, H.-R.; Tsai, B.-S.; Liu, H.-C. Insight on Creep Behavior for Arrayed Interphase Nano-Precipitation in Ti-Microalloyed HSLA Steel. *Mater. Chem. Phys.* **2020**, *255*, 123553. [[CrossRef](#)]
21. Cong, J.; Li, J.; Fan, J.; Liu, P.; Misra, R.D.K.; Shang, C.; Wang, X. The Impact of Interphase Precipitation on the Mechanical Behavior of Fire-Resistant Steels at an Elevated Temperature. *Materials* **2020**, *13*, 4294. [[CrossRef](#)] [[PubMed](#)]
22. Krbata, M.; Krizan, D.; Eckert, M.; Kaar, S.; Dubec, A.; Ciger, R. Austenite Decomposition of a Lean Medium Mn Steel Suitable for Quenching and Partitioning Process: Comparison of CCT and DCCT Diagram and Their Microstructural Changes. *Materials* **2022**, *15*, 1753. [[CrossRef](#)]
23. Chih-Yuan, C.; Shih-Fan, C.; Chien-Chon, C.; Jer-Ren, Y. Control of Precipitation Morphology in the Novel HSLA Steel. *Mater. Sci. Eng. A* **2015**, *634*, 123–133. [[CrossRef](#)]
24. Chen, C.-Y.; Yang, J.-R.; Chen, C.-C.; Chen, S.-F. Microstructural Characterization and Strengthening Behavior of Nanometer Sized Carbides in Ti–Mo Microalloyed Steels during Continuous Cooling Process. *Mater. Charact.* **2016**, *114*, 18–29. [[CrossRef](#)]
25. Brytan, Z.; Król, M.; Benedyk, M.; Pakieła, W.; Tański, T.; Dagnaw, M.J.; Snopiński, P.; Pagáč, M.; Czech, A. Microstructural and Mechanical Properties of Novel Co-Free Maraging Steel M789 Prepared by Additive Manufacturing. *Materials* **2022**, *15*, 1734. [[CrossRef](#)]
26. E28 Committee ASTM International. *Test Methods for Elevated Temperature Tension Tests of Metallic Materials*; ASTM International: West Conshohocken, PA, USA, 2009.
27. Jang, J.H.; Lee, C.-H.; Heo, Y.-U.; Suh, D.-W. Stability of (Ti, M)C (M = Nb, V, Mo and W) Carbide in Steels Using First-Principles Calculations. *Acta Mater.* **2012**, *60*, 208–217. [[CrossRef](#)]
28. Cong, J.; Li, J.; Fan, J.; Misra, R.D.K.; Xu, X.; Wang, X. Effect of Austenitic State before Ferrite Transformation on the Mechanical Behavior at an Elevated Temperature for Seismic-Resistant and Fire-Resistant Constructional Steel. *J. Mater. Res. Technol.* **2021**, *13*, 1220–1229. [[CrossRef](#)]
29. Honeycombe, R.W.K.; Mehl, R.F. Transformation from Austenite in Alloy Steels. *Met. Trans. A* **1976**, *7*, 915–936. [[CrossRef](#)]
30. Lifshitz, I.M.; Slyozov, V.V. The Kinetics of Precipitation from Supersaturated Solid Solutions. *J. Phys. Chem. Solids* **1961**, *19*, 35–50. [[CrossRef](#)]
31. Dunlop, G.L.; Honeycombe, R.K.W. The Role of Dislocations in the Coarsening of Carbide Particles Dispersed in Ferrite. *Philos. Mag.* **1975**, *32*, 61–72. [[CrossRef](#)]
32. Ardell, A.J. On the Coarsening of Grain Boundary Precipitates. *Acta Metall.* **1972**, *20*, 601–609. [[CrossRef](#)]
33. Deschamps, A.; Hutchinson, C.R. Precipitation Kinetics in Metallic Alloys: Experiments and Modeling. *Acta Mater.* **2021**, *220*, 117338. [[CrossRef](#)]

34. Gladman, T. Precipitation Hardening in Metals. *Mater. Sci. Technol.* **1999**, *15*, 30–36. [[CrossRef](#)]
35. Lu, S.-L.; Yang, S.-C.; Zhu, K.; Chen, Y.-S.; Cairney, J.M.; Lin, C.-M.; Yen, H.-W. Strategy of Complex Carbides in Microalloyed 4Mn Steels Processed by Quenching and Austenite Reversion. *Mater. Des.* **2023**, *230*, 111951. [[CrossRef](#)]

Disclaimer/Publisher’s Note: The statements, opinions and data contained in all publications are solely those of the individual author(s) and contributor(s) and not of MDPI and/or the editor(s). MDPI and/or the editor(s) disclaim responsibility for any injury to people or property resulting from any ideas, methods, instructions or products referred to in the content.